Smart Structures and Systems, *Vol. 15, No. 4 (2015) 1085-1101*
DOI: http://dx.doi.org/10.12989/sss.2015.15.4.1085

Characterization of railway substructure using a hybrid cone penetrometer

Yong-Hoon Byun[a], Won-Taek Hong[b] and Jong-Sub Lee[*]

School of Civil, Environmental and Architectural Engineering, Korea University, 145, Anam-ro, Sungbuk-gu, Seoul, 136-713, Korea

(Received March 17, 2014, Revised July 10, 2014, Accepted August 20, 2014)

Abstract. Changes in substructure conditions, such as ballast fouling and subgrade settlement may cause the railway quality deterioration, including the differential geometry of the rails. The objective of this study is to develop and apply a hybrid cone penetrometer (HCP) to characterize the railway substructure. The HCP consists of an outer rod and an inner mini cone, which can dynamically and statically penetrate the ballast and the subgrade, respectively. An accelerometer and four strain gauges are installed at the head of the outer rod and four strain gauges are attached at the tip of the inner mini cone. In the ballast, the outer rod provides a dynamic cone penetration index (DCPI) and the corrected DCPI (CDCPI) with the energy transferred into the rod head. Then, the inner mini cone is pushed to estimate the strength of the subgrade from the cone tip resistance. Laboratory application tests are performed on the specimen, which is prepared with gravel and sandy soil. In addition, the HCP is applied in the field and compared with the standard dynamic cone penetration test. The results from the laboratory and the field tests show that the cone tip resistance is inversely proportional to the CDCPI. Furthermore, in the subgrade, the HCP produces a high-resolution profile of the cone tip resistance and a profile of the CDCPI in the ballast. This study suggests that the dynamic and static penetration tests using the HCP may be useful for characterizing the railway substructure.

Keywords: cone tip resistance; dynamic cone penetration index; dynamic cone penetrometer; mini cone; railway substructure

1. Introduction

Railway track systems play an important role in sustaining an economy, particularly in moving imports and exports, shipments of fossil fuels, and passenger service. The performance of the railway track system is mainly influenced by the interaction between the superstructure and the substructure. The substructure, consisting of the ballast, the sub-ballast, and the subgrade, is implicitly concerned, whereas the superstructure components such as rails, sleepers, and fasteners are relatively well defined. Although expensive remedial works continue to be carried out, the cause of track-quality deterioration related to the substructure condition often remains undiagnosed (Selig and Waters 1994).

*Corresponding author, Professor, E-mail: jongsub@korea.ac.kr
[a] Postdoctoral Fellow
[b] Ph.D. Student

http://www.techno-press.org/?journal=sss&subpage=8 ISSN: 1738-1584 (Print), 1738-1991 (Online)

The ballast, which is placed on top part of the substructure, provides resistance to the vertical, lateral, and longitudinal forces generated by traffic loading. The sub-ballast between the ballast and the subgrade prevents interpenetration and allows the water to be drained. The subgrade provides stability to the ballast and sub-ballast and influences the track performance such as the elastic deflection of the rail, the deterioration of the sleeper and the ballast, and the differential settlement of the rails. In the subgrade, the stresses imposed by repeated dynamic loading may cause the soil to be pressed to the side and upward of the track. The so-called "progressive shear failure" mostly occurs in the top layer of the subgrade within a depth of 1 m (Chrismer and Li 1997). The progressive shear of the subgrade may cause track geometry changes.

A series of in-situ test devices have been investigated to review the applicability of the methods to the railway substructure (Brough *et al.* 2003, Brough *et al.* 2006). Trial pit excavation is a traditional method used to investigate the ballast depth and the subgrade condition, but it has a significant potential to destroy the railway. An automatic ballast sampler has also been used to obtain a more detailed profile of the substructure. However, the sample obtained by boring is usually highly disturbed and cannot exhibit the representative characteristics of the substructure. The dynamic cone penetrometer (DCP) has been developed to evaluate the in-situ strength of granular materials. In particular, using a correlation between the DCP index (DCPI) and the California bearing ratio (CBR), the dynamic cone penetrometer has been applied to design, construct, and maintain the road pavement (Kleyn and Savage 1982, Siekmeier *et al.* 2000, Mohammadi *et al.* 2008). Because of the differences in the penetration mechanism, the DCPI correlation with resilient modulus is poor, whereas the DCPI-CBR correlation presents high reliability. As a nondestructive test device, the portable falling weight deflectometer (PFWD) is widely adapted to evaluate pavements because of its quick measurement and high performance. However, the PFWD can only be used to estimate the elastic modulus in homogeneously layered media (Asli *et al.* 2012). The ground penetrating radar (GPR) can produce a continuous profile of the substructure for anomaly identification without engineering properties (Sussmann *et al.* 2003, Al-Qadi *et al.* 2010).

The static cone penetration test (CPT), which is commonly performed using a standard cone penetrometer with a diameter of 35.7 mm, can provide cone tip resistance and sleeve friction in order to evaluate the strength and the bearing capacity. The cone tip resistance can be correlated with the resilient modulus of the railway subgrade, which is related to the subgrade settlement. In addition, the magnitude of the cone tip resistance determines whether the progressive shear failure occurs. For the CPT, the resolution of the cone tip resistance depends on the size of the cone penetrometer. The resolution of the cone tip resistance increases when the diameter of the cone penetrometer decreases because of the dimension of the disturbed zone (Hird *et al.* 2003, Hird and Springman 2006). Kurup and Tumay (1998, 1999) applied a miniature cone penetrometer with a diameter of 16.0 mm to the subgrade on a highway. Unlike the highway environment, the in-situ tests on the railway must assess the substructure without eliminating or disturbing the substructure components. In particular, the application of the miniature cone penetrometer is difficult for the ballast layer because the ballast has a much greater diameter than the miniature cone penetrometer (Bolton *et al.* 1999). Therefore, a new in-situ testing technique is required to evaluate the condition of the railway substructure, which considers the railway environment.

This paper presents the development and application of the hybrid cone penetrometer (HCP) to characterize the railway substructure. The HCP consists of an outer rod and an inner mini cone that can be used in the dynamic and static penetration tests, respectively. This paper demonstrates the design of the HCP, the dynamic and static calibrations, and the test procedures. Laboratory tests

and field application tests are then discussed.

2. Hybrid Cone Penetrometer (HCP)

Static and dynamic penetration methods have been used for subsurface characterization in numerous in-situ tests. In the static cone penetration test (CPT) and the California bearing ratio (CBR) test, the penetrometers are statically pushed. The static penetration methods have a high resolution in order to detect variations in soil strength. Note that for static penetration, the penetrometers require a high reaction load such as a reaction frame anchored into the ground or heavy equipment. However, in the standard penetration test (SPT) and the dynamic cone penetration (DCP) test, the penetrometers are dynamically impacted by dropping a hammer. The dynamic penetration method produces a high penetration capacity using lightweight devices. However, analysis using the dynamic penetration method is much more complicated than that using the static penetration method.

The conventional in-situ testing methods that use static or dynamic penetration were not sufficient to provide consistent and accurate characterization of the railway substructure. Furthermore, a new testing method that can be performed with minimal disturbance in the railway substructure is required. Therefore, the hybrid cone penetrometer (HCP), which is applicable to static and dynamic penetration methods, was developed in this study.

2.1 Shape

The HCP is fundamentally a cone penetrometer composed of an outer rod and an inner mini cone. The outer rod and the inner mini cone of the HCP were designed to have different outer diameters ($D_{outer\ rod}$= 24 mm and $D_{inner\ rod}$= 15 mm), as shown in Fig. 1. Note that the outer diameter of the cone tip is greater ($D_{cone\ tip}$= 20 mm) than the diameter of the inner rod in order to prevent the cone tip from entering the inside of the outer rod and to reduce the sleeve friction. An accelerometer (PCB, 350B03) and four strain gauges (Kyowa, 120 Ω) were mounted on the head of the outer rod to monitor the energy transferred from the impact hammer as shown in Figs. 1(a) and 1(b). For the dynamic penetration, a donut-type hammer and a hammer guide were coupled to the outer rod as shown in Fig. 1(a). Fig. 1(c) shows the shape of the inner mini cone, which includes four strain gauges used to measure the cone tip resistance. To push the inner mini cone, the combination of an electric motor and a reaction frame was used.

The strain gauges and the accelerometer in the HCP were connected with a data acquisition system as shown in Fig. 2. The data acquisition system was composed of a bridge box and a data logger (HBM, MX410), which could record a dynamic response and a static resistance with a sampling rate of 1 to 100 kHz. To improve the application of the HCP, the data acquisition system adopted in this study was compacted into simple devices, compared with a previous study by Byun *et al*. (2014).

2.2 Mechanical force calibration

The mechanical forces at the rod head and the cone tip were measured using the strain gauges. A force calibration was performed to develop a relationship between the mechanical force and the output voltage. Using a loading frame, a series of loads was applied to the outer rod and the inner

mini cone of the HCP. Considering the difference in cross-sectional area, a greater maximum load was applied to the outer rod than to the inner mini cone. A full-bridge circuit was used, which can amplify the change in the output voltage by loading and compensate the temperature change. In the full-bridge circuit, the output voltage only depends on the loading, assuming that the input voltage and the gauge factor are constant (for details, refer to Yoon and Lee 2012). Furthermore, Yoon and Lee (2012) reported that the mini cone configured with the full-bridge circuit produced more reliable results than that configured with the half-bridge circuit because the full-bridge circuit effectively compensates for the temperature change (Shin *et al.* 2009, Yoon *et al.* 2011, Lee *et al.* 2013). During the calibration, the input voltage of 1.25 V and the temperature of 20 ℃ remained constant for the determination of reliable calibration results. The applied mechanical force versus the measured output voltage from the strain gauges is plotted in Fig. 3. Fig. 3 shows that the correlations between the mechanical forces and the output voltage are greater than 0.99 in the outer rod and the inner mini cone. Note that the output voltage of the inner mini cone increases more sharply than that of the outer rod because the inner mini cone has a smaller cross-sectional area.

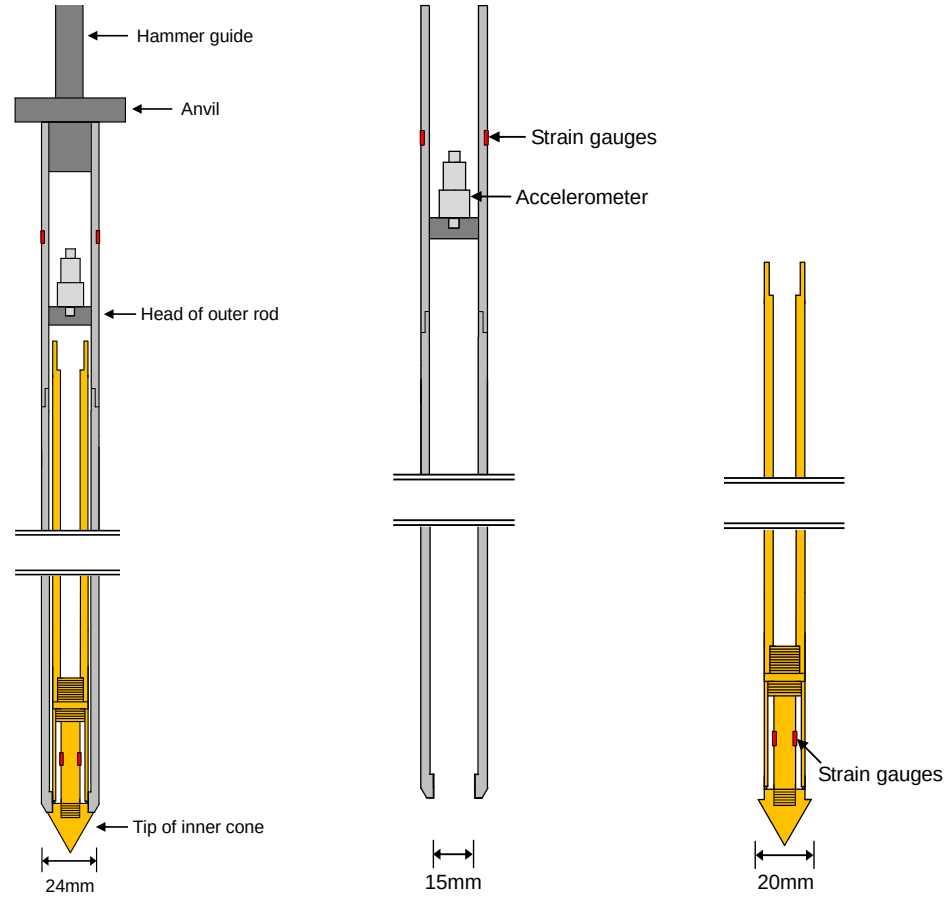

(a) Whole (b) Outer rod (c) Inner mini cone

Fig. 1 Schematic drawing of the hybrid cone penetrometer

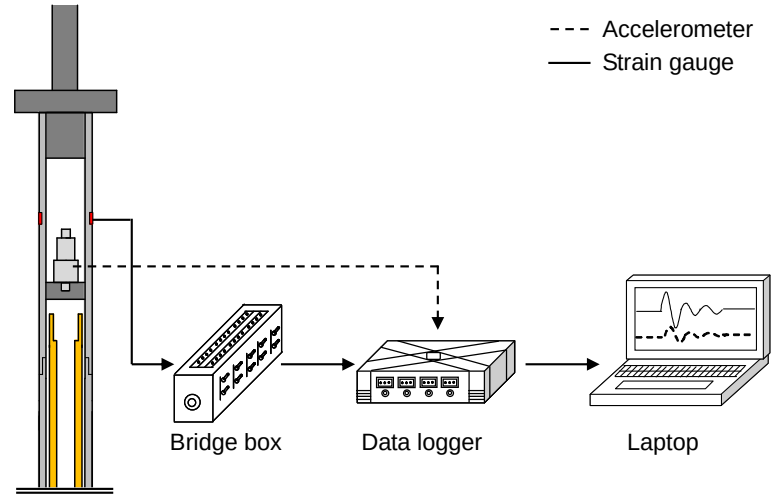

(a) Dynamic penetration

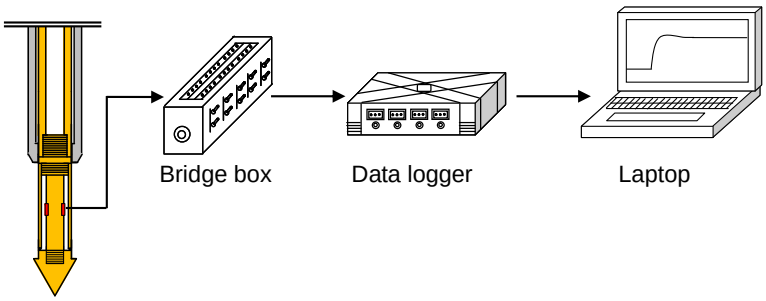

(b) Static penetration

Fig. 2 Measurement system of the hybrid cone penetrometer

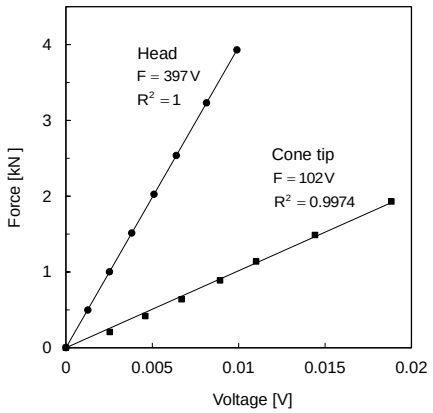

Fig. 3 Mechanical force calibration for the strain gauges

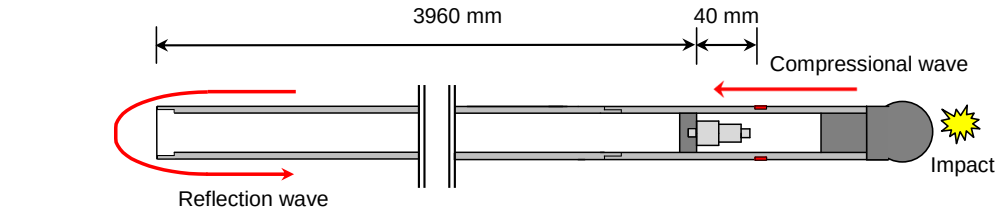

(a) Schematic drawing of the experiment

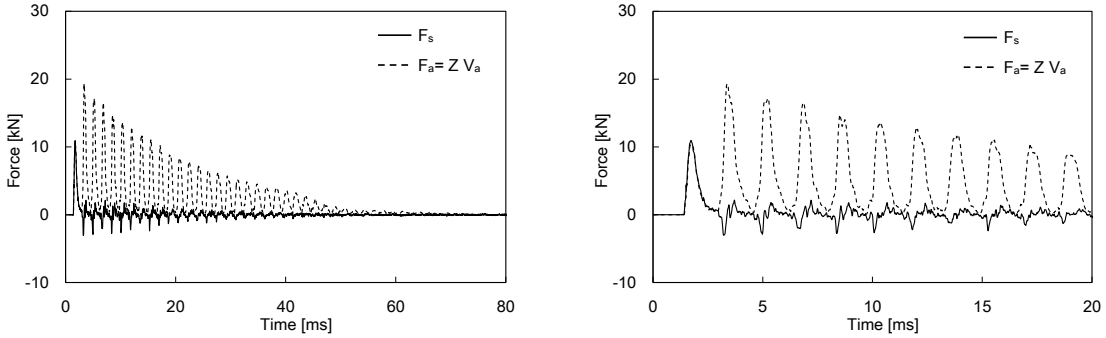

(b) Response results on a scale of 80 ms

(c) Response results on a scale of 20 ms

Fig. 4 Investigation of dynamic response of the accelerometer installed at the outer rod

*F_s: force measured by strain gauges; F_a: force determined by accelerometer; V_a: velocity calculated from acceleration; Z: impedance of outer rod

2.3 Investigation of dynamic response

The dynamic responses at the rod head were detected using the accelerometer and the strain gauges to estimate the energy transferred to the rod head. The acceleration measured from the accelerometer was integrated to obtain the velocity. The velocity multiplied by the impedance of the outer rod (Z) can then be represented in terms of force as follows

$$F_a = ZV_a = \frac{EA}{C}V_a \tag{1}$$

where F_a and V_a are the force and the velocity, respectively, calculated from the acceleration. E, A, and C represent the elastic modulus, the cross-sectional area, and the compressional wave speed of the outer rod, respectively. To determine the transferred energy, the force measured from the strain gauges and the velocity calculated by integrating the acceleration were used (ASTM D4633).

For the free-end condition without resistance, the force estimated by the velocity should match the force measured by the strain gauges until the reflection waves are detected. To verify the performance of the accelerometer and strain gauge, an investigation of dynamic response was conducted with an extended outer rod, which was hung using several strings. The extended outer rod, which consists of the head of the outer rod and four additional rods with a total length of 400 cm, was impacted by a pendulum weight of 52 N that fell from a height of 8 cm (see Fig. 4(a)).

The force signals measured at the rod head are plotted in Fig. 4. Fig. 4 shows the attenuation of the force signals during the multi-reflection process. In the initial stage, the force measured by the strain gauges was similar to that estimated by the velocity. However, after 2.97 ms, the force estimated by the velocity was almost twice that measured by the strain gauges. Note that the time of 2.97 ms is exactly identical to the arrival time of the reflection wave from the other side of the extended outer rod. Considering the free-end condition, the velocity of the compressional wave at the end of the bar is twice that along the bar (Umeda and Ueda 1990).

2.4 Test procedure

The procedures of the dynamic and static penetration tests are shown in Fig. 5 and are described as follows:

1) Two guide plates, which can sustain the verticality of the HCP, are located on the railroad ties as shown in Fig. 5(a).
2) The HCP with the hammer and the guide is placed in the holes of the guide plates. Then, the HCP is dynamically penetrated by the impact of the hammer as shown in Fig. 5(b). As the penetration proceeds, the guide plates move down as the cone is advanced.
3) After the tip of the HCP reaches the top of the subgrade, the hammer and the guide plates are removed. The electric motor combined with the reaction frame is placed to statically penetrate the inner mini cone as shown in Fig. 5(c).
4) Before the static penetration, the HCP should be slightly extracted to ensure the zero loading state. The outer rod of the HCP, which plays the role of a casing inserted in the ballast layer, ensures the verticality of the inner mini cone during the static penetration.
5) The inner mini cone is statically pushed into the subgrade as shown in Fig. 5(d). The penetration rate is maintained at 1 mm/sec.

3. Laboratory tests

The laboratory tests were performed in a chamber to apply the HCP under fully controlled conditions. Dynamic and static cone penetration tests using the HCP were performed in the chamber. In addition, a dynamic cone penetration (DCP) test was performed using a standard dynamic cone penetrometer.

3.1 Materials and specimen preparation

Two types of materials, gravel and sandy soil, were used to model the ballast and the subgrade, respectively. The particle sizes of the gravel were analyzed by washing and sieving following ASTM C136. The median grain size (D_{50}) of the gravel is 42 mm; the gradation and the uniformity coefficient of the gravel are 1.09 and 1.63, respectively, which indicates that the gravel is uniformly graded without fine particles. For the sandy soil, a specific gravity of 2.65 was measured by using a pycnometer; the sieve and the hydrometer analysis were conducted to determine the grain size distribution. Based on the Unified Soil Classification System, the sandy soil is classified as SW. The index properties of the sandy soil are summarized in Table 1.

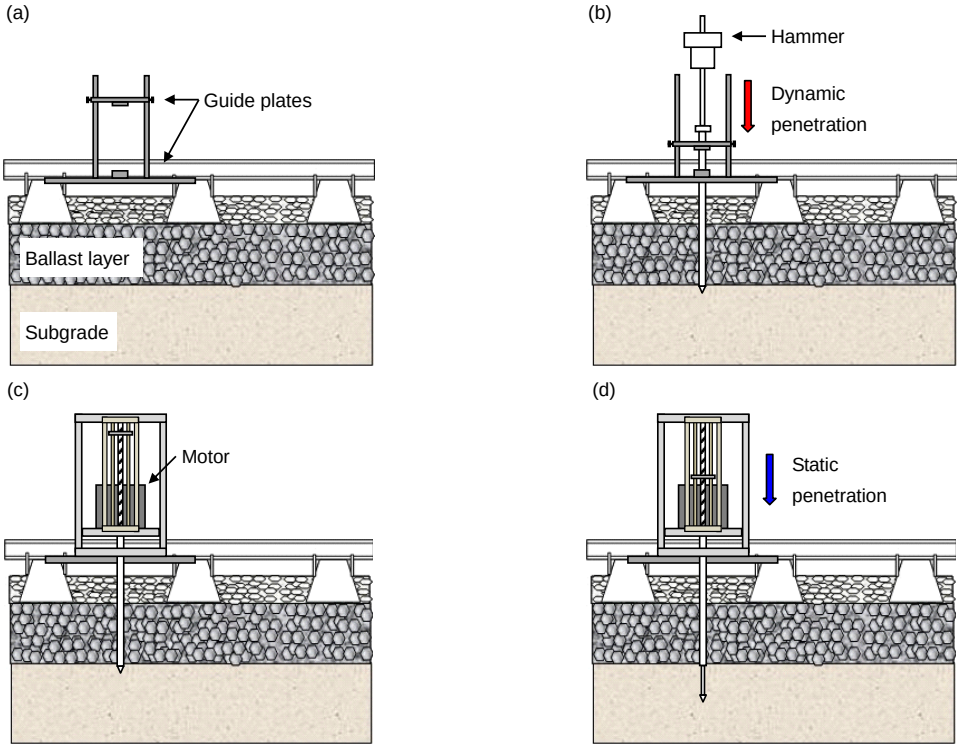

Fig. 5 Test procedures: (a) set-up of the guide plates, (b) dynamic penetration of the HCP by the hammer impact, (c) connection of an electric motor and (d) static penetration of the inner mini cone

The gravel and the sandy soil were oven-dried and subsequently prepared in a square-shaped chamber. Fig. 6 shows a schematic view and the inner dimensions of the chamber (length and width = 750 mm, height = 1000 mm). Dried soil was deposited in the chamber in four distinct layers. To maintain uniform compactive effort, each layer was compacted using a hammer with a weight of 68.6 N and a falling height of 500 mm. After the compaction in each layer was complete, the soil surface was leveled. The representative relative density in the sandy soil was evaluated as 63% from the average height of the specimen and the weight of the sandy soils. The gravel was then placed on the surface of the sandy soil. Using the same type of compaction control, five discrete layers of the gravel were compacted.

Table 1 Engineering properties of sandy soil

Specific gravity G_s	Median diameter D_{50} [mm]	Curvature coefficient C_c	Uniformity coefficient C_u	Maximum void ratio e_{max}	Minimum void ratio e_{min}	USCS
2.65	1.36	1.16	10.94	0.78	0.42	SW

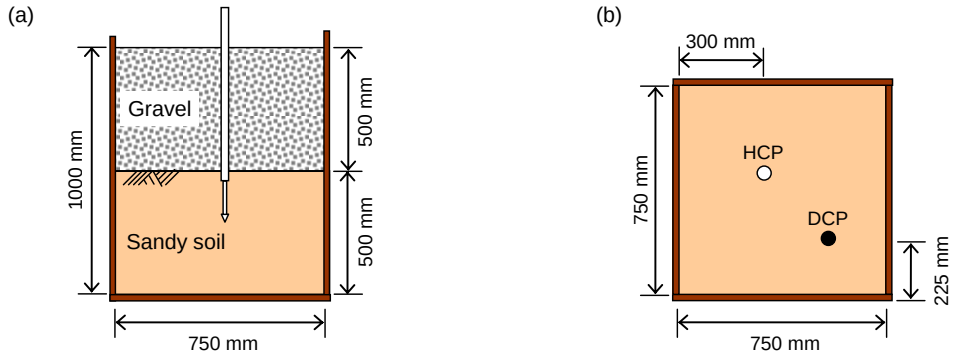

Fig. 6 Schematic drawing of the railway substructure model: (a) side view and (b) top view

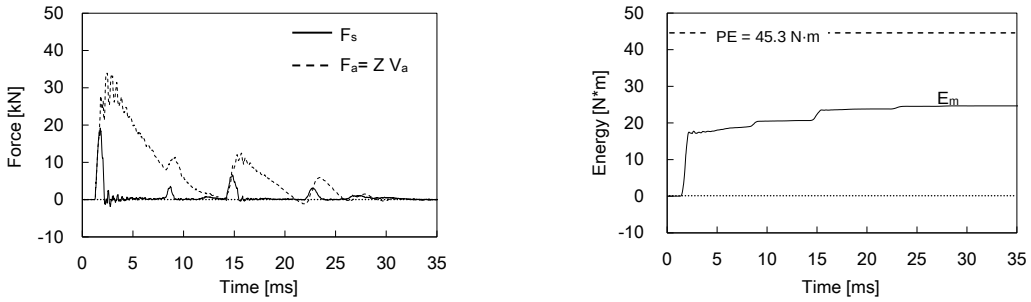

(a) Force-time waveform (b) Energy-time waveform

Fig. 7 Measured dynamic responses at the penetration depth of 210 mm

*PE: potential energy of the drop hammer; E_m: transferred energies into the rod head

3.2 Force and velocity responses

The force and the velocity at the rod head of the HCP were measured by strain gauges and an accelerometer to evaluate the transferred energy. Typical force and velocity signatures detected at the penetration depth of 210 mm are plotted in Fig. 7(a). Fig. 7(a) shows that the peak of the force calculated from the acceleration is slightly smaller than twice that obtained from the strain gauges. Note that the penetration of the HCP produces the sleeve friction and the reflection wave reduces the particle velocity compared to the dynamic response at the free-end condition.

The energies transferred into the rod head can be evaluated using the F-V integration method (ASTM D4633) as follows.

$$E = \int F_s V_a dt \tag{2}$$

where F_s is the force obtained from the strain gauges and V_a is the velocity calculated from the acceleration. Based on the F-V integration method, at a depth of 210 mm, the energy transferred into the rod head is plotted in Fig. 7(b). Fig. 7(b) shows that the potential energy and the transferred energy are 45.3 N·m and 24.6 N·m, respectively. Note that the average energy transferred into the rod head is approximately 22.8 N·m along the depth.

3.3 Dynamic penetration index of HCP

Dynamic cone penetration tests using the HCP were performed on the specimen with the gravel layers. During the DCP tests, the number of blows is recorded at each penetration depth, and the DCP index (DCPI) can be calculated as follows (Embacher 2006).

$$DCPI = \frac{P_{n+1} - P_n}{B_{n+1} - B_n} \tag{3}$$

where P and B are the penetration depth and the blows at the $(n)^{th}$ or $(n+1)^{th}$ drop of the hammer, respectively. The DCPI represents the characteristics of the materials at each depth. To obtain the representative value of the materials, the averaged DCPI can be used for a given depth (Mohammadi *et al.* 2008). In this study, the DCPI was averaged at every third depth measurement to characterize the variation of the penetration resistance and to reduce the deviation from the mean DCPI. Fig. 8(a) shows the profiles of the DCPI and the averaged DCPI that was obtained by the HCP. In the DCPI profiles, the initial penetration depth of 140 mm corresponding to the seating drops of the HCP was excluded. In the previous studies, the first two blows of the hammer were not included in the DCPI calculation in order to minimize the vertical confinement effect (Dai and Kremer 2006, Siekmeier *et al.* 2009). In the gravel layer, the DCPI decreases with an increase in depth. Note that the vertical confinement effect decreases with an increase in depth through the transition zone, which ranges from the depth of 210 mm to 450 mm (see also Webster *et al.* 1994).

To compensate the effect of variations in the transferred energy, the DCPI can be corrected by measuring the transferred energy into the rod head. In the case of SPT, the standard rod energy ratio of 60% between the transferred energy into the rod head and the potential energy of the hammer has been suggested. For the laboratory test in this study, the average rod energy ratio is approximately 51%, as shown in Fig. 8(b). Therefore, the corrected DCPI with the transferred energy can be defined as follows.

$$CDCPI = DCPI \times \frac{E_{50}}{E_m} \tag{4}$$

where CDCPI is the corrected DCPI, E_{50} is half the potential energy of the hammer, and E_m is the energy measured at each blow. Note that, in the case of the donut-type hammer in SPT, the average rod energy ratio of 50% has been generally proposed (Skempton 1986). Fig. 8(c) shows the CDCPI profile. As the penetration depth increases, the CDCPI decreases, and the CDCPI attains the minimum value at the interlayer between the gravel and the sandy soil. The results demonstrate that the gravel and the sandy soil were mixed at the interlayer, and the higher density at the interlayer causes the higher CDCPI. To verify the repeatability of the HCP, several DCP tests were performed at the same specimen. The profiles of the DCPI, rod energy ratio, and CDCPI were almost identical for all tests. Thus, in the same specimen, the results of the DCP tests using the HCP were considered as repeatable.

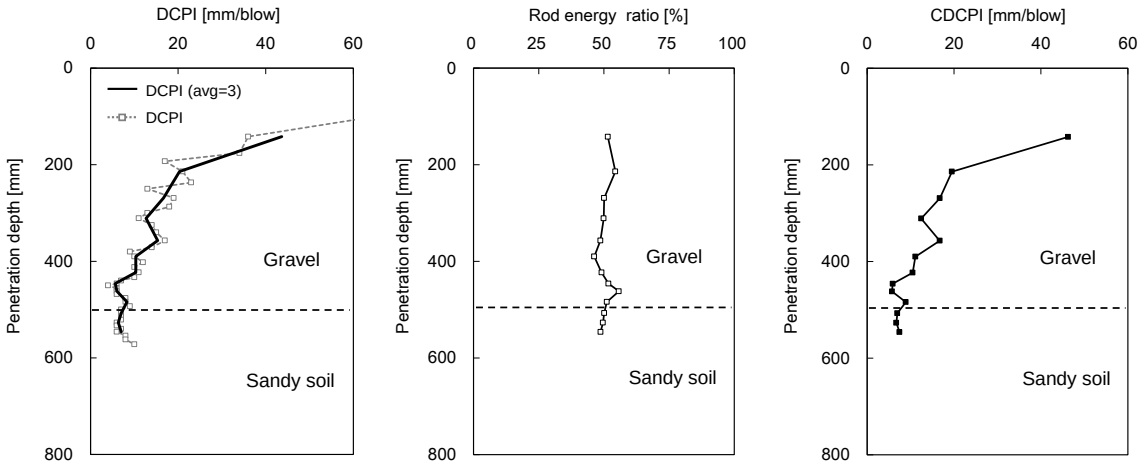

(a) DCPI (b) Rod energy ratio (c) CDCPI

Fig. 8 Results of the dynamic cone penetration test using the HCP in the chamber

3.4 Static cone tip resistance of HCP

The static cone penetration test using the inner mini cone of the HCP was performed for the sandy soil. The inner mini cone ($D_{cone\ tip}$ = 20 mm) was pushed through the depth of 570 to 920 mm at a penetration rate of 1 mm/sec. The penetration rate was selected for the higher resolution of the cone tip resistance and the drainage condition (for details refer to Byun *et al.* 2013). To measure the cone tip resistance, a constant input voltage of 1.25 V was applied to the strain gauges installed in the cone tip, and the temperature of the specimen was maintained at 10℃. In previous studies, the response of the strain gauges applied with an input voltage of 1-2 V remained constant (Lee *et al*. 2009, Yoon and Lee 2012). The profile of the static cone tip resistance (q_c) measured by the inner mini cone of the HCP in sandy soil is plotted in Fig. 9(a). In addition, the CDCPI values obtained in the gravel layer are plotted in Fig. 9(a). Fig. 9(a) shows that the cone tip resistance dramatically increases with an increase in depth from 570 to 640 mm. The constant cone tip resistance of 4.1 MPa is then maintained from the depth of 640 to 750 mm. At the depth of greater than 750 mm, the cone tip resistance increases along the depth because of the stress level effect of the accumulated compactive effort (Bolton *et al.* 1999).

3.5 Standard DCP test

A standard DCP test was performed to compare with the results of the cone penetration tests using the HCP. Fig. 9(b) shows the DCPI profile of the standard DCP from the gravel layer to the sandy soil layer. The dotted line and the solid line indicate the DCPI profiles recorded at every blow and averaged with three blows, respectively. For the gravel layer, the evolution of the DCPI recorded at every blow fluctuated more along the depth than that averaged with three blows. Note that the standard DCP has a primary disadvantage for large granular materials with a high degree of variability, which is related to the maximum size of the granular materials and the amount of

fines (Ayers and Thompson 1988). The fluctuation of the DCPI in the gravel layer is more dominant than that of the CDCPI of the HCP. The absence of guide plates and the difference in diameters between the cone tip and the rod may affect the verticality of the DCP. In turn, the verticality of the DCP causes the DCPI to fluctuate. The DCPI is lower than expected at the interface of the gravel and the sandy soil layers. In the sandy soil, the DCPI is approximately 24.5 mm/blow. Previously reported values of the well-graded sands (SW) sampled in Korea ranged from 6.0 to 10.3 mm/blow (Kim et al. 2006). Note that the dry unit weight of the specimen (γ = 17.1 kN/m^3) in this study is lower than that (γ = 18.9 - 20.3 kN/m^3) reported by Kim *et al.* (2006).

3.6 Correlation between CDCPI and q_c

The dynamic and static cone penetration tests using the HCP provide the profiles of the corrected dynamic cone penetration index (CDCPI) and the cone tip resistance (q_c). To clarify the relation between the CDCPI and the cone tip resistance, a series of dynamic and static cone penetration tests using the HCP were performed in the chamber filled with sandy soil. The sandy soil was compacted for a relative density of 63%, 76%, 84%, and 97%. In each specimen with a certain relative density, a dynamic penetration test and a static penetration test were performed using the outer rod and the inner mini cone of the HCP, respectively. Note that the average cone tip resistance and average CDCPI were estimated at the depth of from 450 to 550 mm. Fig. 10 shows the relationship between the cone tip resistance and the CDCPI. The CDCPI decreases as the cone tip resistance increases with a high reliability. Thus, the HCP can provide a continuous profile through the composite layer in order to obtain the variation of soil strength.

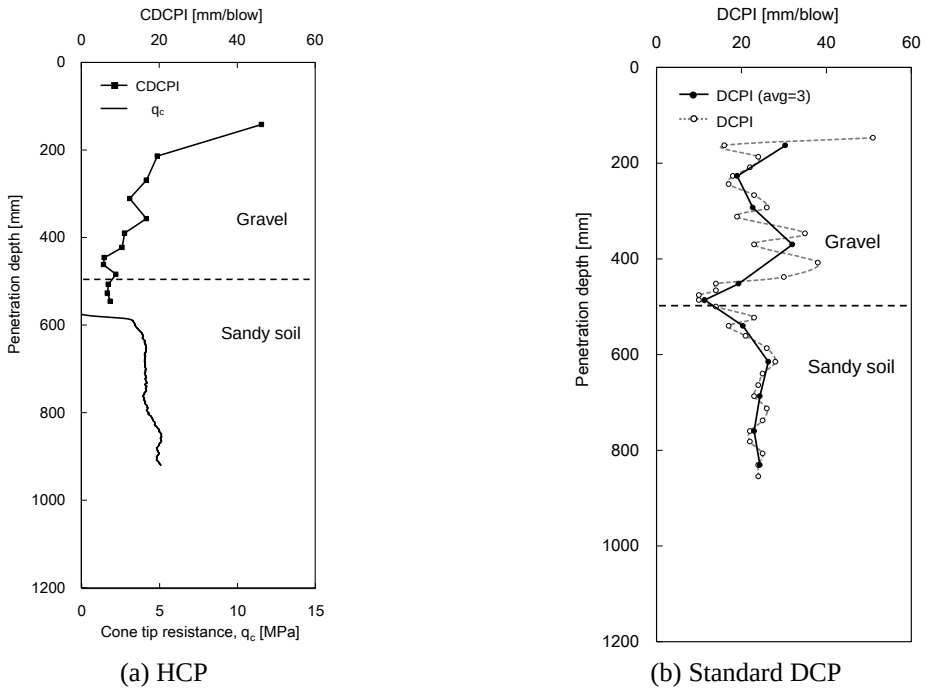

(a) HCP (b) Standard DCP

Fig. 9 Comparison of test results using two cone penetrometers in the chamber

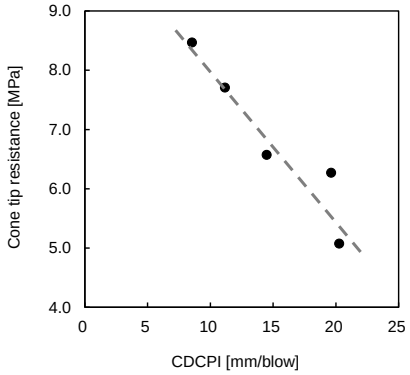

Fig. 10 Correlation between the cone tip resistance and the CDCPI in the sandy soil

4. Field application tests

The field application tests were performed on a railway near Korea University in Seoul. As the previously mentioned test procedure, the dynamic and static cone penetration tests using the HCP were carried out and compared with the standard DCP test.

4.1 Dynamic penetration index of HCP

The dynamic cone penetration test using the HCP was conducted in the field up to a penetration depth of 660 mm. The results of the dynamic cone penetration test are plotted in Fig. 11. To exclude the initial blows as seating drops, the DPI was recorded from the depth of 130 mm. The DCPI decreases up to the depth of 260 mm and subsequently slightly increases up to the depth of 370 mm. The average DCPI of 4.7 mm/blow is maintained at the depth of from 370 to 470 mm. The DCPI then increases with an increase in depth until it is 10.5 mm/blow at the depth of 660 mm. Based on the energy transferred to the rod head, the rod energy ratios along the depth are plotted in Fig. 11(b). The average rod energy ratio is approximately 48% for the entire depth. The corrected dynamic cone penetration index (CDCPI) with the transferred energy at each depth is plotted in Fig. 11(c). The CDCPI obtained in the field test was smaller and more stable than that in the laboratory test. Note that the ballast layer in the field contained a high percentage of fines, which originated from ballast breakdown, sleeper wear, and subgrade infiltration. The CDCPI profile, which is independent of the transferred energy, clearly represents a more reliable variation of soil strength than that of the DCPI.

4.2 Static cone tip resistance of HCP

The static cone penetration test was performed after confirming the DCPI increase, which indicated that the tip of the HCP reached the subgrade layer. The inner mini cone of the HCP was pushed from 650 to 1140 mm. The profile of the cone tip resistance with the CDCPI along the penetration depth is plotted in Fig. 12(a). The cone tip resistance initially increases up to the depth of 660 mm and subsequently remains at approximately 5.0 MPa up to the depth of 870 mm. As the

penetration depth increases, the cone tip resistance evolves to a maximum of 6.5 MPa and gradually stabilizes to approximately 5.7 MPa.

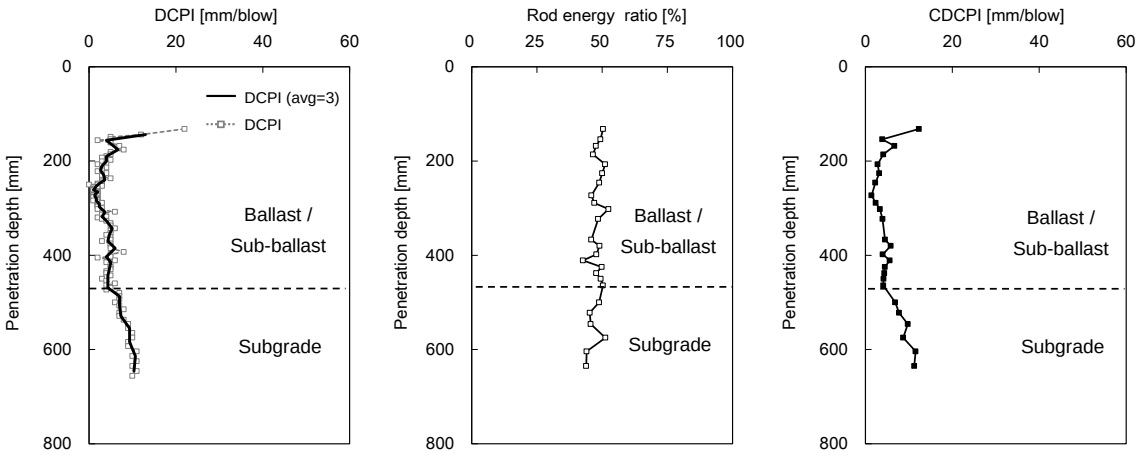

(a) DCPI (b) Rod energy ratio (c) CDCPI

Fig. 11 Results of the dynamic cone penetration test using the HCP in the field

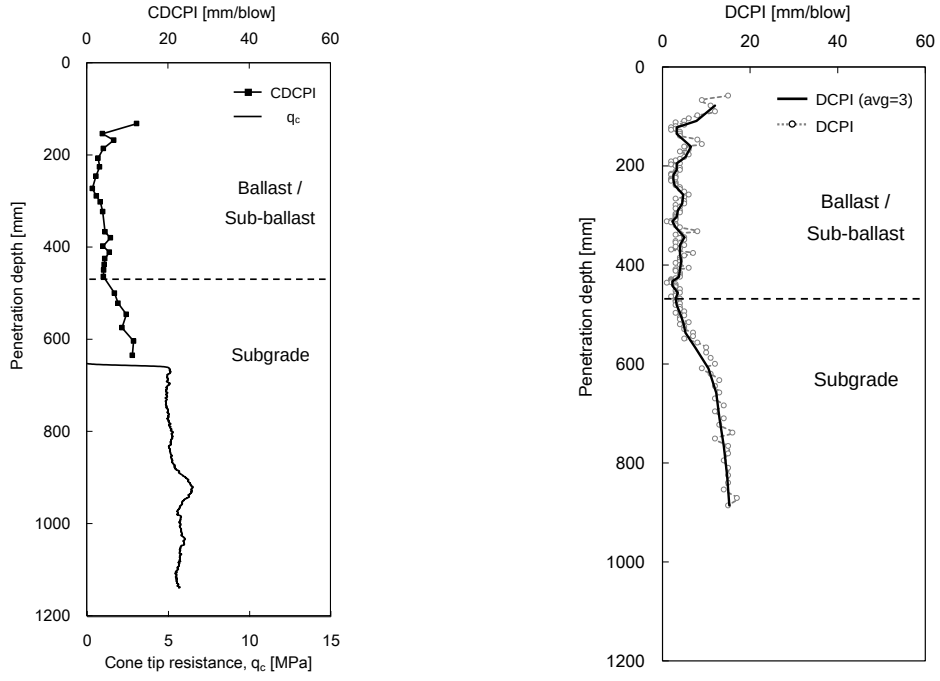

(a) HCP (b) Standard DCP

Fig. 12 Comparison of test results using two cone penetrometers in the field

4.3 Standard DCP test

A standard DCP test was conducted near the position applied by the HCP. The DCPI profile of the standard DCP is plotted in Fig. 12(b). The DCPI at the depth of from 120 to 470 mm remains constant with a small fluctuation. The DCPI then gradually increases with an increase in depth up to the depth of 890 mm. Using the standard DCP, the substructure profile obtained by the HCP was reconfirmed. Based on the results of Webster *et al.* (1994) in an identical test section, the cone tip resistance range of from 6.2 to 7.2 MPa corresponds to the DCPI range of from 11 to 17 mm/blow. In conclusion, the field test results demonstrate that the HCP more effectively characterizes the railway substructure and can clearly detect the variation of soil strength in the subgrade.

5. Conclusions

The hybrid cone penetrometer (HCP) was developed to evaluate railway substructures based on the dynamic and static penetration tests. The HCP consists of an outer rod and an inner mini cone for the dynamic and static penetrations, respectively. The outer rod of the HCP, which contained an accelerometer and four strain gauges at the head, was used for the measurement of the dynamic response during dynamic penetration in the ballast. The measured dynamic cone penetration index (DCPI) was corrected with the energy transferred into the rod head (defined as CDCPI). To estimate a static cone tip resistance in the subgrade, four strain gauges were installed at the tip of the inner mini cone. The results of mechanical force calibration for the strain gauges showed a strong correlation between the mechanical force and the output voltage. In addition, the dynamic responses of the accelerometer and the strain gauges were well matched. According to the test procedure of the HCP, the outer rod was penetrated through the ballast by using a hammer, and the inner mini cone was then statically pushed into the subgrade at a constant penetration rate.

The dynamic and static cone penetration tests were performed in the specimen prepared with gravel and sandy soil to apply the HCP under fully controlled conditions. In the gravel layer, the evolution of the DCPI obtained from the HCP fluctuated less than that obtained from the standard DCP. For the sandy soil, several laboratory tests using the HCP showed that the cone tip resistance measured in the static cone penetration test was inversely proportional to the CDCPI measured in the dynamic cone penetration test.

The field tests were performed in an abandoned railway in Seoul. In the ballast, the dynamic cone penetration tests provided the CDCPI profile, which is corrected for the effect of variations in the transferred energy. Furthermore, the CDCPI profile clearly represents the more rational variation of soil strength than that of the DCPI. On the other hand, in the subgrade, the inner mini cone of the HCP produced a high-resolution profile of the cone tip resistance. This study demonstrates that the HCP may be effectively used to characterize the railway substructure with minimal disturbance in the ballast, the sub-ballast, and the subgrade layers.

Acknowledgments

This work was supported by the National Research Foundation of Korea (NRF) grant funded by the Korea government (MSIP) (NRF-2011-0018110).

References

Al-Qadi, I.L., Xie, W., Roberts, R. and Leng, Z. (2010), "Data analysis techniques for GPR used for assessing railroad ballast in high radio-frequency environment", *J. Transp. Eng.- ASCE*, **136**(4), 392-399.

Asli, C., Feng, Z.Q., Porcher, G. and Rincent, J.J. (2012), "Back-calculation of elastic modulus of soil and subgrade from portable falling weight deflectometer measurements", *Eng. Struct.*, **34**, 1-7.

ASTM C136 (2006), *Sieve Analysis of Fine and Coarse Aggregates*, *Annual Book of ASTM Standard*, **04.02**, ASTM International, West Conshohocken, PA.

ASTM D4633 (2005), *Standard test method for energy measurement for dynamic penetrometers*, Annual Book of ASTM Standard, **04.08**, ASTM International, West Conshohocken, PA.

Ayers, M.E. and Thompson, M.R. (1988), *Rapid shear strength evaluation of in situ ballast/subballast materials*, Department of Civil Engineering, University of Illinois at Urbana-Champaign, Technical report submitted to USA-CERL, June.

Bolton, M.D., Gui, M.W., Garnier, J., Corte, J.F., Bagge, G., Laue, J. and Renzi, R. (1999), "Centrifuge cone penetration tests in sand", *Geotechnique*, **49**(4), 543-552.

Brough, M.J., Ghataora, G.S., Stirling, A.B., Madelin, K.B., Rogers, C.D.F. and Chapman, D.N. (2003), "Investigation of railway track subgrade. I: In-situ assessment", *Proceedings of the ICE-Transport*, **156**(3), 145-154.

Brough, M.J., Ghataora, G.S., Stirling, A.B., Madelin, K.B., Rogers, C.D.F. and Chapman, D.N. (2006), "Investigation of railway track subgrade. Part 2: Case study", *Proceedings of the ICE-Transport*, **159**(2), 83-92.

Byun, Y.H., Kim, J.H. and Lee, J.S. (2013), "Cone penetrometer with a helical-type outer screw rod for evaluation of the condition of a railway roadbed", *J. Transp. Eng.- ASCE*, **139**(2), 115-122.

Byun, Y.H., Yoon, H.K., Kim, Y.S., Hong, S.S. and Lee, J.S. (2014), "Active layer characterization by instrumented dynamic cone penetrometer in Ny-alesund, Svalbard", *Cold Region Science and Technology*, Elsevier (Submitted).

Chrismer, S.M. and Li, D. (1997), "Cone penetrometer testing for track substructure design and assessment", *Proceedings of the 6th International Heavy Haul Conference: Strategies Beyond 2000*, South Africa.

Dai, S. and Kremer, C. (2006), *Improvement and validation of Mn/DOT DCP specifications for aggregate base materials and select granular* (No. MN/RC-2005-32).

Embacher, R.A. (2006), "Duration of spring thaw recovery for aggregate-surfaced roads", *Transport. Res. Record: J. Transport. Res. Board*, **1967**(1), 27-35.

Hird, C.C. and Springman, S.M. (2006), "Comparative performance of $5cm^2$ and $10cm^2$ piezocones in a lacustrine clay", *Geotechnique*, **56**(6), 427-438.

Hird, C.C., Johnson, P. and Sills, G.C. (2003), "Performance of miniature piezocones in thinly layered soils", *Geotechnique*, **53**(10), 885-900.

Kim, B.I., Jeon, S.I. and Lee, M.S. (2006), "Comparison of Field Bearing Capacity Tests to Evaluate the Field Application of Dynamic Cone Penetrometer Test", *Int J. Highway Eng.*, **8**(4), 75-85.

Kleyn, E.G. and Savage, P.F. (1982), "Application of the pavement DCP to determine the bearing properties and performance of road pavements", *Proceedings of the International Symposium on Bearing Capacity of roads and Airfields*, Trondheim, Norway, June.

Kurup, P.U. and Tumay, M.T. (1998), "Calibration of a miniature cone penetrometer for highway applications", *Transport. Res. Record: J. Transport. Res. Board*, **1614**(1), 8-14.

Kurup, P.U. and Tumay, M.T. (1999), "Continuous intrusion miniature cone penetration test system for transportation applications", *Transport. Res. Record: J. Transport. Res. Board*, **1652**(1), 228-235.

Lee, C., Kim, R., Lee, J.S. and Lee, W. (2013), "Quantitative assessment of temperature effect on cone resistance", *Bull. Eng. Geology Environ.*, **72**, 3-13.

Lee, W.J., Shin, D.H., Yoon, H.K. and Lee, J.S. (2009), "Micro-cone penetrometer for more concise subsurface layer detection", *Geotech. Test. J.*, **32**(4), 358-364.

Mohammadi, S.D., Nikoudel, M.R., Rahimi, H. and Khamehchiyan, M. (2008), "Application of the dynamic

cone penetrometer (DCP) for determination of the engineering parameters of sandy soils", *Geology*, **101**, 195-203.
Selig, E.T., and Waters, J.M. (1994), *Track geotechnology and substructure management*, Thomas Telford.
Shin, D.H., Lee, C., Lee, J.S. and Lee, W. (2009), "Detection of smear zone using micro-cone and electrical resistance probe", *Can. Geotech. J.*, **46**(6), 719-726.
Siekmeier, J.A., Young, D. and Beberg, D. (2000), "Comparison of the dynamic cone penetrometer with other tests during subgrade and granular base characterization in Minnesota", *ASTM Special Technical Publication*, **1375**, 175-188.
Siekmeier, J., Pinta, C., Merth, S., Jensen, J., Davich, P., Camargo, F. and Beyer, M. (2009), *Using the dynamic cone penetrometer and light weight deflectometer for construction quality assurance* (No. MN/RC 2009-12).
Skempton, A.W. (1986), "Standard penetration test procedures and the effects in sands of overburden pressure, relative density, particle size, ageing and overconsolidation", *Geotechnique*, **36**(3), 425-447.
Sussmann, T.R., Selig, E.T. and Hyslip, J.P. (2003), "Railway track condition indicators from ground penetrating radar", *NDT & E Int.*, **36**(3), 157-167.
Webster, S.L., Brown, R.W. and Porter, J.R. (1994), *Force projection site evaluation using the electric cone penetrometer (ECP) and the dynamic cone penetrometer (DCP)* (No. WES/TR/GL-94-17), Army Engineer Waterways Experiment Station Vicksburg Ms Geotechnical Lab.
Yoon, H.K., Jung, S.H. and Lee, J.S. (2011), "Characterisation of subsurface spatial variability using a cone resistivity penetrometer", *Soil Dyn. Earthq. Eng.*, **31** (7), 1064-1071.
Yoon, H.K. and Lee, J.S. (2012), "Micro cones configured with full-bridge circuits", *Soil Dyn. Earthq. Eng.*, **41**, 119-127.

CC